JACS
JOURNAL OF THE AMERICAN CHEMICAL SOCIETY
Article
pubs.acs.org/JACS

Thermally Activated Delayed Fluorescence of Fluorescein Derivative for Time-Resolved and Confocal Fluorescence Imaging

Xiaoqing Xiong,[†] Fengling Song,*[,†] Jingyun Wang,[‡] Yukang Zhang,[†] Yingying Xue,[†] Liangliang Sun,[†] Na Jiang,[†] Pan Gao,[‡] Lu Tian,[§] and Xiaojun Peng[†]

State Key Laboratory of Fine Chemicals, Dalian University of Technology, 2 Linggong Road, Dalian 116024, People's Republic of China

Supporting Information

ABSTRACT: Compared with fluorescence imaging utilizing fluorophores whose lifetimes are in the order of nanoseconds, time-resolved fluorescence microscopy has more advantages in monitoring target fluorescence. In this work, compound **DCF-MPYM**, which is based on a fluorescein derivative, showed long-lived luminescence (22.11 μs in deaerated ethanol) and was used in time-resolved fluorescence imaging in living cells. Both nanosecond time-resolved transient difference absorption spectra and time-correlated single-photon counting (TCSPC) were employed to explain the long lifetime of the compound, which is rare in pure organic fluorophores without rare earth metals and heavy atoms. A mechanism of thermally activated delayed fluorescence (TADF) that considers the long wavelength fluorescence, large Stokes shift, and long-lived triplet state of **DCF-MPYM** was proposed. The energy gap (ΔE_{ST}) of **DCF-MPYM** between the singlet and triplet state was determined to be 28.36 meV by the decay rate of DF as a function of temperature. The ΔE_{ST} was small enough to allow efficient intersystem crossing (ISC) and reverse ISC, leading to efficient TADF at room temperature. The straightforward synthesis of **DCF-MPYM** and wide availability of its starting materials contribute to the excellent potential of the compound to replace luminescent lanthanide complexes in future time-resolved imaging technologies.

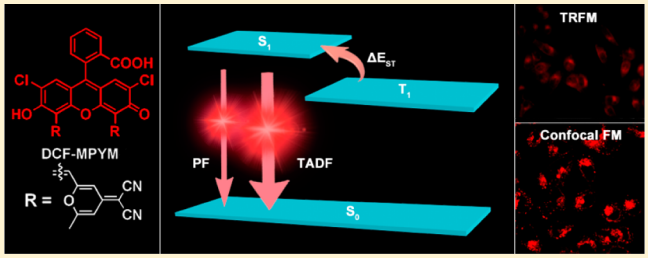

1. INTRODUCTION

Fluorescence imaging is a powerful and widely used method for complex biological environments because of its characteristic features, which include high sensitivity, high spatial resolution, and ease of use; this technology is important for elucidating biological functions.[1] Compared with fluorescence imaging utilizing fluorophores whose lifetimes are in the order of nanoseconds, time-resolved fluorescence microscopy exploits advantages in monitoring target fluorescence.[1a] Introduction of an appropriate delay time between the pulsed excitation light and measurement of the long-lived luminescence of dyes is expected to allow imaging with eliminating the short-lived background fluorescence and provide high signal-to-noise ratios.[2] Heavy-metal complexes showing metal-to-ligand charge transfer (MLCT) luminescence are good candidates for time-resolved fluorescence imaging because of their relatively long lifetimes (microseconds (μs) and milliseconds (ms));[3] these complexes show many other advantageous photophysical properties for bioimaging, such as large Stokes shifts for easy distinction between excitation and emission.[4] In recent years, many luminescent terbium,[2f,5] europium,[4,9,10] and iridium[13,16] complexes have been reported to be applicable in staining cells. However, these compounds often transfer the energy of the excited triplet state to surrounding cells and tissues through singlet oxygen, thereby acting as photosensitizers and resulting in cell death via apoptosis or necrosis as well as photo bleaching of the dyes.[1a,6] Extensive studies on luminescent lanthanide complexes have been performed, but few complexes have been employed for time-resolved fluorescence imaging. In particular, the toxicity of these heavy metal-based complexes must be considered in practical applications.

Many of the organic fluorescent dyes have been reported to be nontoxic to cells, but these typical organic fluorescent dyes possess the drawback of having short fluorescence lifetimes in the nanosecond range.[7] Thus, conventional small-molecule organic dyes cannot eliminate most autofluorescence backgrounds from biological samples. To extend the lifetime of fluorescent dyes and ameliorate the toxic effects of heavy-metal complexes on cells, new organic fluorescent dyes with long fluorescence lifetime are necessary. Delayed fluorescence (DF) continues to be a rare phenomenon observed in organic fluorophores and metal complexes.[8] DF has a spectrum similar to that of prompt fluorescence (PF) but a substantially longer lifetime because the population of the excited singlet state originates from the triplet state.[9] DF can be divided into three types, namely: E-type DF (the fluorescence from the first singlet excited state (S_1), which becomes populated by a reverse intersystem crossing (RISC) from the triplet excited state (T_1), that is, thermally activated delayed fluorescence);[10] P-type DF

Received: March 6, 2014
Published: June 17, 2014

   dx.doi.org/10.1021/ja502292p | J. Am. Chem. Soc. 2014, 136, 9590−9597

(triplet−triplet annihilation);[11] and recombination fluorescence (recombination of radical ions or opposite charges).[12] Eosin, a fluorescein derivative, was one of the first organic fluorophores found to exhibit E-type DF, but later, the studies on fluoresceins with DF remain limited.[13]

In our present work, we synthesized a fluorescein derivative with E-type DF based on our previous work[14] by introducing a similar up-conversion mechanism from the triplet to the singlet excited state without using heavy-metal complexes. The structure of the fluorescein derivative is shown in Scheme 1.

Scheme 1. Structure of DCF-MPYM Dye

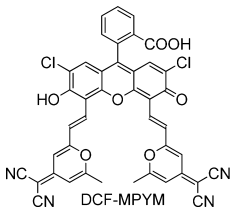

We investigate the derivative using steady-state photoluminescence measurements, transient absorption techniques in the nanosecond time scale, time-resolved photoluminescence measurements, and fluorescence lifetimes techniques. The delayed fluorescence at room temperature makes the derivative possess long-lived luminescence. Because its lifetime is on the order of microseconds, the derivative has been found useful in time-resolved fluorescence imaging. The particular properties including a long luminescence lifetime and large Stoke shift make this fluorescein derivative have potential to replace luminescent lanthanide complexes in time-resolved imaging.

2. RESULTS AND DISCUSSION

2.1. Molecular Design and Synthesis of DCF-MPYM. The literature reported that aromatic carbonyls exhibit some degree of spin−orbit coupling at the carbonyl oxygen that allows for intrinsic triplet generation through intersystem crossing.[15] This characteristic makes aromatic carbonyls unique among light-element organic compounds even though they do not normally provide bright or, in many cases, detectable phosphorescence.[16] The fluorescence intensity of fluorescein molecules reportedly decreases by introduction of a substituent to the xanthene moiety because of the accelerated intersystem crossing (ISC) from the excited singlet state to triplet state.[17] So we utilized the Duff reaction and Knoevenagel condensation to synthesize the 2′,7′-dichlorofluorescein (DCF) derivative **DCF-MPYM** as previously reported.[14] We expect that this derivative can produce triplet states.

The photophysical property of **DCF-MPYM** was characterized in our reported literature (see Supporting Information Figure S1).[14] **DCF-MPYM** has two absorption peaks and two emission peaks in ethanol, but we did not provid a reasonable explanation for this phenomenon. **DCF-MPYM** has a Stokes shift (>150 nm), which is substantially larger than that of conventional DCF. Conventional DCF has a small (20−30 nm) Stokes shift. Here, we speculate that the large Stokes shift may be attributed to an excited triplet state in **DCF-MPYM**.

2.2. Nanosecond Time-Resolved Transient Difference Absorption Spectrum of DCF-MPYM. The nanosecond time-resolved transient difference absorption spectra have been reported to investigate the characteristics of triplet states.[18] The nanosecond time-resolved transient difference absorption spectra of **DCF-MPYM** (10.0 μM) were obtained (Figure 1). Upon pulsed laser excitation at 532 nm, significant bleaching

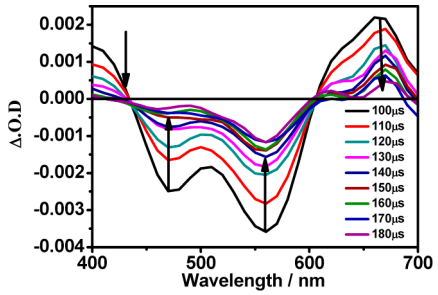

Figure 1. Nanosecond time-resolved transient difference absorption spectra of **DCF-MPYM** with different delay time (10.0 μM in deaerated ethanol, λ_{ex} = 532 nm).

peaks were observed at 400, 480, 555, and 650 nm, respectively (Figure 1). Bleaching at 480 and 555 nm are caused by depletion of the ground state of the compound. Transient absorption bands at about 400 and 650 nm may be attributed to the transient absorption of the triplet excited state of **DCF-MPYM** considering the fact that the bleaching processes are in microsecond scale. In fact, the decay lifetimes of the two transients at 480 and 650 nm were 23.64 and 23.89 μs in deaerated ethanol, respectively (Figure 2). The microsecond scale lifetimes of the transients indicate that long-lived triplet excited states are achieved upon visible-light excitation.

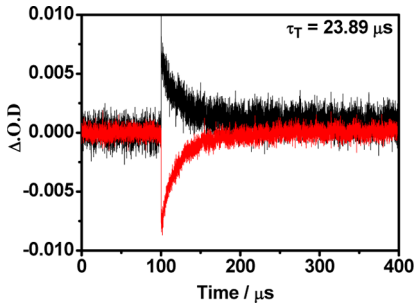

Figure 2. Decay trace of triplet state (monitored at 650 nm, black line) and restoration of bleaching ground state (monitored at 480 nm, red line). All measurements are performed in Ar-saturated solution and the concentration of **DCF-MPYM** is 10.0 μM in deaerated ethanol.

2.3. Luminescence Spectra. Next, we aim to clarify whether the existed long-lived triplet excited states decay through radiation or nonradiation. The normalized steady-state fluorescence spectrum (Figure 3, black line) and time-resolved fluorescence spectrum (Figure 3, red line) of **DCF-MPYM** were obtained at room temperature under air and argon atmosphere, respectively. The weak short-wavelength emission (around 525 nm) in steady-state spectrum disappeared in the time-resolved fluorescence spectrum with a 100 μs delay. And the maximum long-wavelength emission around 651 nm in the time-resolved fluorescence spectrum unexpectedly agreed closely with the maximum at 649 nm in the steady-state fluorescence spectrum with a 2 nm red-shift.

Then, we try to prove that the emission at 651 nm in the time-resolved fluorescence spectrum is related to the triplet excited states. Ethyl iodide was added to a solution of **DCF-MPYM** in nitrogen-saturated CH_3CN, the heavy atom effect is expected to increase the lowest triplet excited state (T_1) yield.[12]

dx.doi.org/10.1021/ja502292p | J. Am. Chem. Soc. 2014, 136, 9590−9597

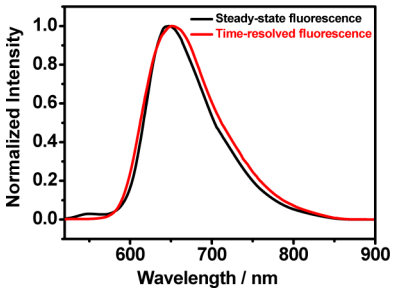

Figure 3. Normalized emission spectra of **DCF-MPYM** (10.0 μM in CH_3CN, λ_{ex} = 485 nm). Black line: Steady-state fluorescence spectrum under air atmosphere (delay time, 0 s). Red line: time-resolved fluorescence spectrum under Ar atmosphere. Delayed detection was carried out in phosphorescence mode (total decay time, 5 ms; delay time, 0.1 ms; gate time, 1.0 ms).

As we expected, the delayed emission at around 651 nm had much enhancement after the addition of ethyl iodide (Supporting Information Figure S2), which results from the T_1 of the derivative **DCF-MPYM**.

As well as known, oxygen is able to quench triplet states.[19] To further clarify whether the delayed emission at 651 nm is associated with the oxygen, we measured the delayed emission spectra of the compound **DCF-MPYM** (10.0 μM in CH_3CN) with and without argon bubbling. The luminescence intensity at 651 nm measured under Ar atmosphere (15.175 a.u.) was much higher than that measured under aerated conditions (0.625 a.u.) (Figure 4). Thus, the fluorescence intensity was

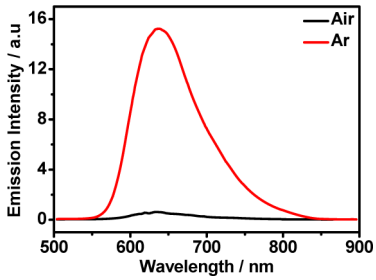

Figure 4. Delayed spectrum of **DCF-MPYM** (10.0 μM in CH_3CN) in air (black line), and delayed spectrum of **DCF-MPYM** (10.0 μM in CH_3CN) under Ar atmosphere (red line). All detections were carried out in phosphorescence mode (total decay time, 5 ms; delay time, 0.1 ms; gate time, 1.0 ms) and under an excitation wavelength of 485 nm.

enhanced by 23-fold by argon purging, whereas the steady-state fluorescence spectra were found no significant changes between Ar and aerated atmosphere (Supporting Information Figure S3). Because DF is known to be more sensitive to oxygen than PF,[20] we can propose that the oxygen-sensitive delayed emission at 651 nm may be thermally activated delayed fluorescence (TADF) from the first excited singlet state, which is obtained through a RISC process from the oxygen-sensitive T_1 state.

Meanwhile, we can explain the reason for 2 nm red-shift between 649 and 651 nm. The observed red-shift phenomenon between steady-state spectrum and time-resolved fluorescence spectrum was also found in other reported TADF systems.[8b,d,21] The phenomenon was explained to be caused by the difference of nuclear configuration between the singlet and triplet excited states in TADF systems.[10e]

2.4. Luminescence Lifetime Measurement. Delayed fluorescence has much longer lifetime than prompt fluorescence, because the population of the excited singlet state originates from a long-lived triplet state.[8a] Specifically, the lifetime of delayed fluorescence is more sensitive to oxygen.[20b,c] To gain better insights into the characteristics of the delayed fluorescence, the luminescence lifetimes at 630 nm were measured by time-correlated single-photon counting (TCSPC) in the nanosecond time scale and in the microsecond time scale. As shown in Supporting Information Table S1, the luminescence lifetime in microsecond time scale has two components in oxygen-free environment with an average lifetime of 22.11 μs. After the oxygen-free sample was settled for 6 h under air atmosphere, the fluorescence lifetime decreased from 22.11 to 4.30 μs (Figure 5).

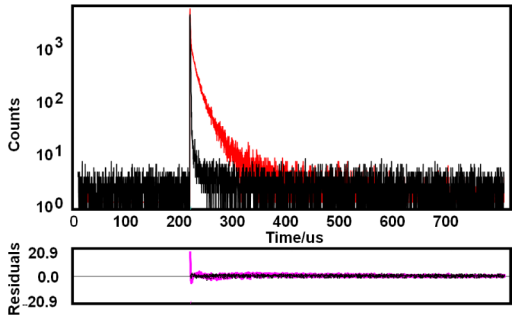

Figure 5. Emission decays of **DCF-MPYM** (10.0 μM) in ethanol at room temperature, red curve shows the profile after deoxygenating (τ = 22.11 μs) and black curve shows the profile after the oxygen-free sample was settled for 6 h under air atmosphere (τ = 4.30 μs). Excited at 485 nm and monitored at 630 nm.

Compared with the delayed component, the prompt component is not sensitive to oxygen. According to the results of the nanosecond time scale lifetime experiment, the fluorescence lifetime of fast decay component at 630 nm was 2.72 ns in oxygen-free environment and the lifetime was 2.79 ns after the oxygen-free sample was settled for 6 h under air atmosphere (Supporting Information Table S2). The emission decay profiles were not affected by oxygen significantly (Supporting Information Figure S4). Similarly, the changes of lifetime at 525 nm were also not obvious between deaerated and aerated condition (Supporting Information Table S2 and Figure S5).

Thus, we observed that the decay at 630 nm included a fast, nanosecond component (PF) followed by a slow, microsecond component (DF). And the nonoxygen sensitive emission at 525 nm composed only conventional PF, which had only a fast, nanosecond decay component. This explanation is also supported by the results of Figure 3 (in CH_3CN). The steady-state fluorescence spectrum (black line) shows weak PF at short-wavelength region (around 525 nm) and strong PF at long-wavelength region (649 nm). In the presence of air, the steady-state spectrum should be predominantly composed of prompt fluorescence[22] because the delayed component at 651 nm is sensitive to oxygen and mostly quenched (Figure 4).

However, the emission at long-wavelength region should be DF predominant and overlapped with PF under oxygen-free atmosphere. Therefore, we estimated the intensity ratio I_{DF}/I_{PF} under Ar atmosphere according to a reported strategy.[8a] An I_{DF}/I_{PF} ratio was calculated as 5.32 for **DCF-MPYM** based on the following equation:

dx.doi.org/10.1021/ja502292p | J. Am. Chem. Soc. 2014, 136, 9590−9597

$$\frac{I_{DF}}{I_{PF}} = \frac{\eta_{DF}}{\eta_{PF}} = \frac{1}{(1/(\eta_{S\to T}\eta_{T\to S} - 1))} \quad (1)$$

where $\eta_{S\to T}$ and $\eta_{T\to S}$ stand for the quantum efficiency of triplet and singlet, respectively. The short lifetime component exhibits two-exponential decay at 630 nm (Supporting Information Table S2) that should arise from ISC ($K_{ISC}^{S\to T}$) and PF (K_{PF}). As we all know, $K_{ISC}^{S\to T}$ is larger than K_{PF}; therefore, we ascribed the shorter decay time to $K_{ISC}^{S\to T}$ and the longer decay time to K_{PF}. The quantum efficiency of triplet formation can be estimated as $\eta_{S\to T} = K_{ISC}^{S\to T}/(K_{PF} + K_{ISC}^{S\to T}) = 84.18\%$ according to the lifetime data of oxygen-free sample at 630 nm in Supporting Information Table S2. The efficiency of triplet to singlet $\eta_{T\to S}$ can be regarded as approximately 100% because both nonradiative and radiative decay rates of the triplet state are much smaller than the reverse ISC rate $K_{ISC}^{T\to S}$. This result suggests that the 630 nm emission band predominantly originates from the DF (84.18% of DF and 15.82% of PF in oxygen-free atmosphere).

2.5. Proposed Mechanism, the Energy Difference Estimation between S_1 and T_1 and Density Functional Theory (DFT) Calculations. To produce efficient thermally activated delayed fluorescence (TADF) and realize reverse ISC even in pure aromatic organic compounds, a small energy difference (ΔE_{ST}) between the excited values of the lowest S_1 and lowest T_1 at a given temperature is necessary.[8d] This small ΔE_{ST} plays a critical role in the efficient formation of the triplet state in the organic fluorophore when it lacks heavy atoms and involves no clear n → π^* transition around the S_1 states.[23] Boltzmann statistics show that the smaller the ΔE_{ST} is, the easier achievement of RISC becomes.[8b−d] To quantitatively evaluate ΔE_{ST}, the activation energy ΔE_{ST} was estimated by the following equation:

$$k_{ISC}^{T\to S} = \overline{k_{ISC}}^{T\to S}\exp(-\Delta E_{ST}/k_B T) \quad (2)$$

where k_B is Boltzmann's constant, T is temperature, and $k_{ISC}^{T\to S}$ is the average rate constant for the adiabatic ISC. Because the lifetime of DF is determined by reverse ISC ($k_{ISC}^{T\to S}$),[8b,c] we use the decay rate of DF to represent $k_{ISC}^{T\to S}$ for ΔE_{ST} estimation. So the temperature-dependent luminescence lifetimes were measured at 630 nm from 77 to 300 K (Supporting Information Table S3). Then the decay rates of DF were ploted as a function of temperature (Figure 6), the red curve obtained is the fitting result based on eq 2. The energy gap between the singlet and triplet states (ΔE_{ST}) was determined to be 28.36 meV, which is a small energy gap for efficient thermally activated DF in comparison with the reported data.[8c]

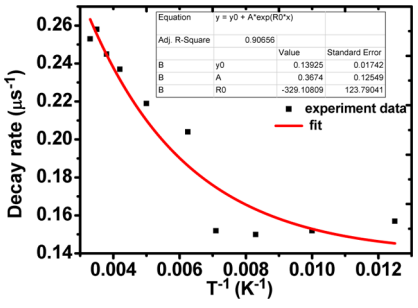

Figure 6. Fluorescence decay rates of **DCF-MPYM** as a function of temperature; fitting is based on eq 2.

To further rationalize the optical properties of compound **DCF-MPYM**, its representative and optimized structure and molecular orbital plots were obtained using density functional theory (DFT) calculations with the B3LYP exchange functional employing the 6-31G(d, p) basis sets using a suite of Gaussian 09 programs. Supporting Information Table S4 summarized the excitation energy calculated for the individual electronic transitions of **DCF-MPYM** in DMSO solvent. As shown in Supporting Information Figure S6, the π-electrons of the LUMO (lowest occupied molecular orbital), HOMO (highest occupied molecular orbital), and HOMO-1 are distributed between pyran nitrile and xanthene moiety. The π-electrons of the HOMO-1 were distributed over the left pyran nitrile and part of the xanthene moiety, the π-electrons of the HOMO were located on the right pyran nitrile as well as part of the xanthene moiety, and the π-electrons of the LUMO concentrated on the xanthene moiety. Such different electronic distributions of the HOMO-1, HOMO, and LUMO lead to the different energies for $S_0 \to S_1$ and $S_0 \to S_4$ transitions. The energies for $S_0 \to S_1$ and $S_0 \to S_4$ transitions are 2.31 eV (537.24 nm) and 2.79 eV (443.97 nm) (Supporting Information Figure S6 and Table S4), respectively, corresponding to the observed two absorption maxima of 569 nm (λ_{ab1}) and 485 nm (λ_{ab2}) (Supporting Information Figure S7). The two absorption bands can be attributed to the dyad structure of **DCF-MPYM.** The peak at 485 nm is assigned to the absorption of xanthene, whereas that of 569 nm is assigned to the extended π-conjugated system combining xanthene and one of pyran nitrile moieties.

As shown in Figure 7, we propose the luminescence mechanism of **DCF-MPYM** based on the above Results and

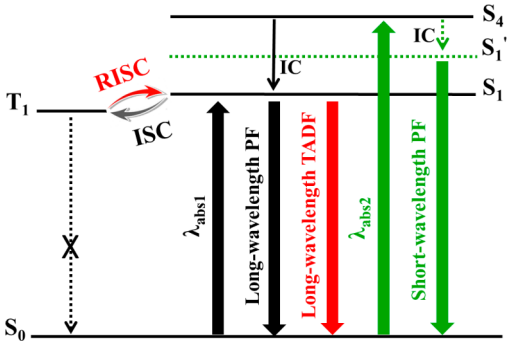

Figure 7. Proposed luminescence mechanism; short-wavelength PF (emission at around 525 nm), long-wavelength PF and TADF (emission at 610−650 nm), and IC (internal conversion).

Discussion. When **DCF-MPYM** is excited at 485 nm (λ_{ab2}), a high energy singlet excited state (S_4) is achieved. A quick internal conversion (IC) process (~10^{-11} s) occurs, which is known to be affected by solvatochromism and hydrogen-bond interaction.[24] According to the emission spectra of **DCF-MPYM** in different solvents (Supporting Information Figure S8), the IC process may lead to the formation of two different lowest singlet excited states (S_1 and S_1'). In protic solvents, the extended π-conjugated system could be distorted because of the possible hydrogen-bond interaction, and a higher energy-level singlet excited state (S_1') may be formed, from which short-wavelength PF (around 525 nm) produces. While in aprotic solvents, the extended π-conjugated system should be predominant during the IC process. The obtained lower level S_1 (compared with S_1') emits long-wavelength PF (610−650

dx.doi.org/10.1021/ja502292p | J. Am. Chem. Soc. 2014, 136, 9590−9597

nm, $S_1 \rightarrow S_0$ transition) as well as gives contributions to TADF (610−650 nm) through ISC and reverse ISC processes.

2.6. Applications of Delayed Fluorescence. Fluorescence dyes are often used as probes in the detection and quantification of analytes. The fluorescence signals of these probes, however, present corresponding disadvantages. Fluorescence dyes suffer from interferences arising from background fluorescence and scattered light. To overcome these disadvantages, many long-wavelength fluorophores have been widely employed, but they have relatively low photo stability, low fluorescence quantum yields, small Stokes shifts and short fluorescence lifetimes. **DCF-MPYM** can overcome these drawbacks of common organic fluorophores, which can be used as a probe in practical applications. The use of long-lifetime emitters is advantageous because time-resolved luminescence detection methods can be employed to remove autofluorescence and scattered lights.[25] Several research groups have demonstrated significant improvements in the signal-to-noise ratio upon implementation of time-resolved discrimination in the detection of long-lifetime signals.[2b−e,g,h] However, long-lifetime pure organic fluorophores that show desirable properties in time-resolved imaging have not been reported.

We previously reported[14] that **DCF-MPYM** could selectively detect BSA in aqueous solutions. To confirm that fluorescence enhancement caused by BSA mainly stems from DF, emission spectra were obtained before and after the addition of BSA (Figure 8). In Figure 8, it shows that only emission at around

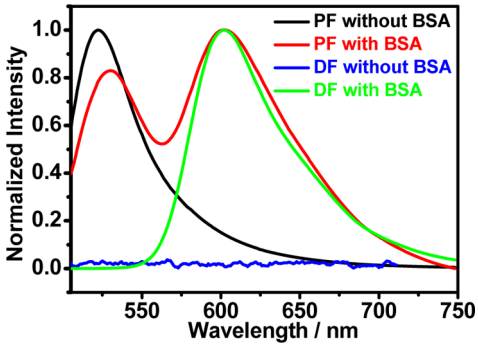

Figure 8. Black line: Normalized steady-state fluorescent spectrum of **DCF-MPYM** (3.0 μM) in PBS (10.0 mM) before addition of BSA. Red line: Normalized steady-state fluorescent spectrum of **DCF-MPYM** (3.0 μM) in PBS (10.0 mM) after addition of BSA. Blue line: Normalized time-resolved spectrum of **DCF-MPYM** (3.0 μM) in PBS (10.0 mM) before addition of BSA; delay time, 0.1 ms. Green line: Normalized time-resolved spectrum of **DCF-MPYM** (3.0 μM) in PBS (10.0 mM); delay time, 0.1 ms. All detections were carried out under air atmosphere and excitation wavelength at 485 nm.

525 nm PF can be observed (black line) prior to the addition of BSA; the emission disappeared after a 100 μs delay (blue line). Maximum emission at 600 nm PF (red line) matched the maximum DF (green line) well after the addition of BSA. The fluorescence lifetime at the long wavelength region (>600 nm) was detected in aqueous solution. Supporting Information Table S5 showed that the total fluorescence lifetime increased with increasing BSA concentration in air condition, and the lifetimes obtained exhibited second-order exponential decay (Supporting Information Figure S9 and Table S5). As shown in Supporting Information Figure S10,[14] **DCF-MPYM** can selectively detect BSA. We have explained the reason for selective detection for BSA that results from the special dyad structure combining DCF and the appropriate appendant. The appendant part has suitable size and polarity, so that **DCF-MPYM** can enter the hydrophobic cavity of BSA. Literature[26] also reported that BSA contains tryptophan, which reacts with singlet oxygen, a known quencher of the DF of fluorophores. Thus, enhancement in DF can be observed after the addition of BSA.

In order to utilize the advantages of long lifetime of **DCF-MPYM**, time-resolved fluorescence imagings were carried out. Bright-field and time-resolved luminescence (excitation of 510−560 nm) images of MCF-7 cancer cells stained by **DCF-MPYM** are shown in Figure 9. Strong red luminescence

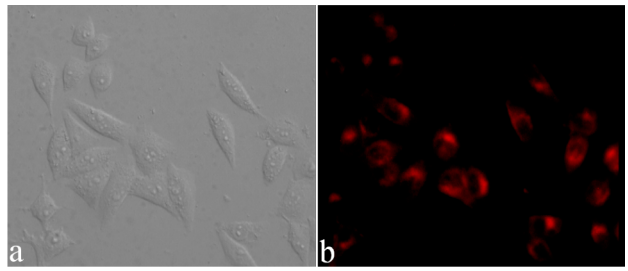

Figure 9. (a) Bright-field and (b) time-resolved luminescence (excitation of 510−560 nm) images of MCF-7 stained with **DCF-MPYM** (20 μM) and BSA (40 μL, 10 mM) at 37 °C. Scale bars = 10 mm.

signals were clearly observed from cells (Figure 9b). Compared with the luminescence images obtained in steady-state mode in Figure 10, the fluorescent image showed much weaker

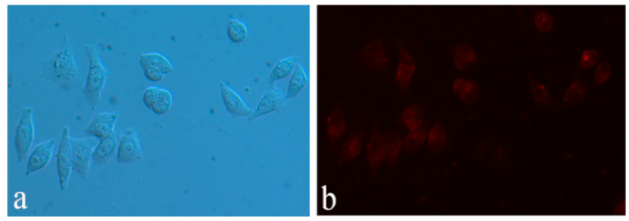

Figure 10. (a) Bright-field, and (b) steady-state luminescence (excitation of 510−560 nm) images of MCF-7 immunostained with **DCF-MPYM** (20 μM) and BSA (40 μL, 10 mM) at 37 °C. Scale bars = 10 mm.

backgrounds in the time-resolved mode (Figure 9). This result indicates that the **DCF-MPYM** can be utilized as a biolabel for visible-light-excited time-resolved luminescence bioimaging applications. In the in vitro experiment, BSA eliminated singlet oxygen and enhanced the intensity of DF (Figure 8). Thus, in living-cell imaging experiments, BSA was added to enhance signals and help the dye penetrate into the cells. **DCF-MPYM** enters the BSA cavity, which can result in more molecules penetrating the membrane then entering the cells. BSA may also quench singlet oxygen in living cells.

Time-resolved luminescence images indicate that **DCF-MPYM** exhibits no obvious organelle staining. Therefore, confocal fluorescence imaging experiments with MCF-7 breast cancer cells were carried out. As shown in Supporting Information Figure S11, the dye permeated the cells' membrane extensively. Fluorescence signals were detected in the cytoplasm rather than in the nuclear region. Morphological

dx.doi.org/10.1021/ja502292p | J. Am. Chem. Soc. 2014, 136, 9590−9597

considerations indicated that the dye localized at lysosomes. To investigate the subcellular localization of **DCF-MPYM** further, the organelle-specific fluorescent dye LysoSensor Green DND-189, a commercial lysosome tracker, was used in colocalization studies. Staining experiments of **DCF-MPYM** were performed with MCF-7 cells and results showed that **DCF-MPYM** colocalized in the lysosome (Figure 11). LysoSensor Green

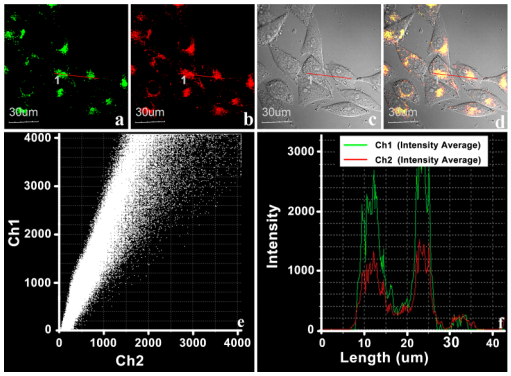

Figure 11. Costaining of **DCF-MPYM** (20.0 μM) with a lysosome-specific dye (200 nM) in MCF-7 cells. (a) Fluorescent image of MCF-7 cells stained with LysoSensor Green DND-189 (λ_{ex} = 488 nm, λ_{em} = 515−545 nm); (b) fluorescent image of MCF-7 cells stained with **DCF-MPYM** (λ_{ex} = 488 nm, λ_{em} = 585−635 nm); (c) bright-field image; (d) merged images of (a), (b), and (c); (e) correlation plot of LysoSensor Green DND-189 and **DCF-MPYM**; (f) intensity profile of ROIs across MCF-7 cells.

showed bright-green fluorescence in channel 1 (Figure 11a), and **DCF-MPYM** showed red fluorescence in channel 2 (Figure 11b). The merged image indicates that the two channels overlap very well, which confirms that **DCF-MPYM** can specifically localize in the lysosomes of living cells (Figure 11d). Changes in the intensity profile of linear regions of interest (ROIs) (**DCF-MPYM** and LysoSensor Green costaining) tended toward synchronization (Figure 11f). The Pearson's coefficient (Rr) of colocalization with LysoSensor Green was found to be 93% in MCF-7 cells. Results of the colocalization study further confirm that **DCF-MPYM** can specifically stain lysosomes. The excitation wavelength used during confocal fluorescence imaging was 488 nm, and the emission wavelength region was 585−635 nm; thus, the emission signals obtained can completely avoid interferences brought about by the excitation wavelength.

Low cytotoxicity of the organic fluorophore is a key criterion for live cell imaging. MTT assays in the MCF-7 cell line were carried out to confirm the low cytotoxicity of **DCF-MPYM**. It shows that the cytotoxicity of **DCF-MPYM** toward the cells at different incubation times was low (Figure 12). Even the cytotoxicity observed at 10 h may be considered moderately low for cells. The low cytotoxicity of **DCF-MPYM** indicates that it can be utilized as a new time-resolved fluorescent dye in living cells to replace luminescent lanthanide complexes with high cytotoxicity.

3. EXPERIMENTAL SECTION

3.1. General Methods. Steady-state fluorescence was measured by a Varian Cary Eclipse fluorescence spectrophotometer (serial no.: FL1109M018). Time-resolved luminescence spectra were obtained using a PerkinElmer LS 50B luminescence spectrometer with the following settings: total

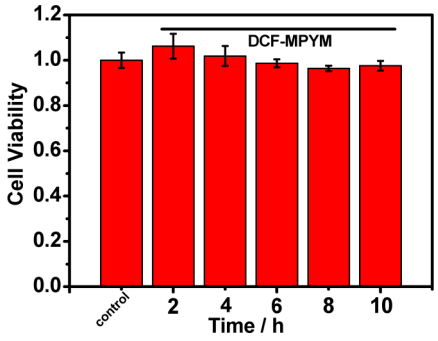

Figure 12. Biological toxicity of MCF-7 cells in the presence of **DCF-MPYM** (20 μM) after different incubation time was determined using the MTT assay by monitoring formazan absorbance at 570 nm. Mean values and standard deviations were obtained from three independent experimental determinations.

decay time, 5 ms; delay time, 0.1 ms; gate time, 1.0 ms; cycle time, 20 ms; excitation and emission slits, 15 nm. Absorption spectra were obtained using a PerkinElmer Lambda35 UV−vis spectrophotometer. Nanosecond time-resolved transient absorption spectra were obtained using an LP920 laser flash photolysis spectrometer (Edinburgh Instruments, U. K.). Nanosecond fluorescence lifetimes were measured using the TCSPC technique on a F900 system with laser excitation at 476.20 nm, and microsecond fluorescence lifetimes were measured by nanosecond pulsed OPO laser synchronized with spectrofluorometer. For the temperature-dependent experiment, the sample was placed in an Optistat DN-V liquid nitrogen cryostat (Oxford, U. K.) with temperatures controlled between 77 and 300 K. The direct detection technique was applied to measure microsecond lifetimes using a photomultiplier tube (PMT, R928). The fluorescence lifetimes of **DCF-MPYM** in aqueous solution before and after the addition of BSA were detected by an LP920 laser flash photolysis spectrometer.

3.2. General Information. Cell imaging measurements were conducted using a spectral confocal microscope (Olympus, FV1000). Time-resolved luminescence imaging measurements were carried out on a laboratory-use luminescence microscope. The microscope—which was equipped with a 30 W xenon flash-lamp (Pulse 300, Photonic Research Systems Ltd.), UV-2A filters (Nikon, excitation filter, 330−380 nm; dichroic mirror, 400 nm; emission filter, > 420 nm), and a time-resolved digital black-and-white CCD camera system (Photonic Research Systems Ltd.)—was used for time-resolved luminescence imaging measurement under the following conditions: delay time, 15 μs; gate time, 100 ms; lamp-pulse width, 6 ms; exposure time, 300 s. Time-resolved luminescence images were pseudo-color-treated using Simple PCI software.

3.3. Cell Culture and Staining. MCF-7 cell lines were cultured in DEME (Invitrogen) supplemented with 10% FCS (Invitrogen). The cells were then stained with **DCF-MPYM** (20 μM) for 120 min at ambient temperature and imaged by confocal fluorescence microscopy and time-resolved fluorescence microscopy. Meanwhile, a total of 40 μL of BSA (10 mM) was added to the system; incubation at 37 °C in 5% CO_2 followed for 2 h. Cells were rinsed three times with clean PBS prior to imaging. For the cell costaining experiment with LysoSensor Green DND-189, pretreated MCF-7 cells were stained with **DCF-MPYM** (20 μM) for 120 min. After rinsing three times with PBS, the same sample was stained with 200

dx.doi.org/10.1021/ja502292p | J. Am. Chem. Soc. 2014, 136, 9590−9597

nM LysoSensor Green DND-189 for 15 min, washed with PBS for three times, and then imaged on confocal microscope (Olympus, FV1000).

3.4. MTT Assay for the Cell Cytotoxicity. This assay involves the reduction of MTT [3-(4,5-dimethylthiazol-2-yl)-2,5-diphenyltetrazolium bromide] tetrazolium to MTT formazan pigment by the metabolic activity of living cells. COS-7 cells were seeded at a density of 1×10^5 cells/mL in a 96-well plate. After 24 h of cell attachment, cells were treated with **DCF-MPYM** at an experimental concentration of 20 μM from 0 to 10 h. After incubation for 2, 4, 6, 8, or 10 h, the medium was removed and cells were washed twice with PBS. MTT tetrazolium solution (100 mL; 0.5 mg/mL in PBS) was added to each well, and the cells were further incubated at 37 °C for 4 h in a 5% CO_2 humidified atmosphere. Excess MTT tetrazolium solution was then carefully removed from the wells, and the colored formazan was dissolved in 100 mL of dimethyl sulfoxide (DMSO). The plate was shaken for 10 min and the absorbance of the solutions in the wells was measured at 600 nm using a microplate reader.

3.5. DCF-MPYM. **DCF-MPYM** was synthesized according to our reported study.[14]

4. SUMMARY

In summary, we have elucidated the luminescence mechanism of a fluorescein derivative **DCF-MPYM**. A long-lived triplet excited state is found and gives red fluorescence around 630 nm. We calculated the energy gap between the singlet and triplet states as 28.36 meV by measuring the decay rate of DF as a function of temperature. The narrow energy gap makes an unusually efficient intersystem crossing occur and results in efficient TADF. The long-lived lifetime of **DCF-MPYM** was used in time-resolved fluorescence cell imaging. It shows good potential as a new time-resolved fluorescence-sensing platform to replace luminescent lanthanide complexes because of its low cytotoxicity.

■ ASSOCIATED CONTENT

Supporting Information

Fluorescence spectra, luminescence lifetime, prompt decays, the DFT calculation results of **DCF-MPYM**, living cell imaging by confocal fluorescence imaging for compound **DCF-MPYM**. This material is available free of charge via the Internet at http://pubs.acs.org.

■ AUTHOR INFORMATION

Corresponding Author

songfl@dlut.edu.cn

Present Addresses

[†]State Key Laboratory of Fine Chemicals, Dalian University of Technology, 2 Linggong Road, Dalian 116024, People's Republic of China.

[‡]School of Life Science and Biotechnology, Dalian University of Technology, 2 Linggong Road, Hi-tech Zone, Dalian 116024, People's Republic of China.

[§]School of Chemistry, Dalian University of Technology, Dalian 116024, People's Republic of China.

Notes

The authors declare no competing financial interest.

■ ACKNOWLEDGMENTS

This work was supported financially by the NSF of China (21222605, 21006009, 21136002, and 21376039), the Fundamental Research Funds for the Central Universities of China, Program for New Century Excellent Talents in University, and the Project-sponsored by SRF for ROCS, SEM. We thank Professor Keli Han from the Dalian Institute of Chemical Physics, Chinese Academy of Sciences for discussion about mechanism of excited states.

■ REFERENCES

(1) (a) Hanaoka, K.; Kikuchi, K.; Kobayashi, S.; Nagano, T. *J. Am. Chem. Soc.* **2007**, *129*, 13502−13509. (b) Nalbant, P.; Hodgson, L.; Kraynov, V.; Toutchkine, A.; Hahn, K. M. *Science* **2004**, *305*, 1615−1619.

(2) (a) Weibel, N.; Charbonnière, L. J.; Guardigli, M.; Roda, A.; Ziessel, R. *J. Am. Chem. Soc.* **2004**, *126*, 4888−4896. (b) Song, B.; Wang, G.; Tan, M.; Yuan, J. *J. Am. Chem. Soc.* **2006**, *128*, 13442−13450. (c) Ye, Z.; Tan, M.; Wang, G.; Yuan, J. *J. Mater. Chem.* **2004**, *14*, 851−856. (d) Song, B.; Wang, G.; Yuan, J. *Chem. Commun.* **2005**, 3553−3555. (e) Xiao, Y.; Zhang, R.; Ye, Z.; Dai, Z.; An, H.; Yuan, J. *Anal. Chem.* **2012**, *84*, 10785−10792. (f) Liu, M.; Ye, Z.; Xin, C.; Yuan, J. *Anal. Chim. Acta* **2013**, *761*, 149−156. (g) Tian, L.; Dai, Z.; Zhang, L.; Zhang, R.; Ye, Z.; Wu, J.; Jin, D.; Yuan, J. *Nanoscale* **2012**, *4*, 3551−3557. (h) Dai, Z.; Tian, L.; Xiao, Y.; Ye, Z.; Zhang, R.; Yuan, J. *J. Mater. Chem. B* **2013**, *1*, 924−927.

(3) Redmond, R. W.; Gamlin, J. N. *Photochem. Photobiol.* **1999**, *70*, 391−475.

(4) (a) Tang, Y.; Yang, H.; Sun, H.; Liu, S.; Wang, J.; Zhao, Q.; Liu, X.; Xu, W.; Li, S.; Huang, W. *Chem.—Eur. J.* **2013**, *19*, 1311−1319. (b) Zhao, Q.; Li, F.; Huang, C. *Chem. Soc. Rev.* **2010**, *39*, 3007−3030. (c) Zhao, Q.; Huang, C.; Li, F. *Chem. Soc. Rev.* **2011**, *40*, 2508−2524. (d) Li, C.; Liu, Y.; Wu, Y.; Sun, Y.; Li, F. *Biomaterials* **2013**, *34*, 1223−1234.

(5) Yuan, J.; Wang, G. *J. Fluoresc.* **2005**, *15*, 559−568.

(6) Gorman, A.; Killoran, J.; O'Shea, C.; Kenna, T.; Gallagher, W. M.; O'Shea, D. F. *J. Am. Chem. Soc.* **2004**, *126*, 10619−10631.

(7) (a) Xiong, X.; Song, F.; Chen, G.; Sun, W.; Wang, J.; Gao, P.; Zhang, Y.; Qiao, B.; Li, W.; Sun, S.; Fan, J.; Peng, X. *Chem.—Eur. J.* **2013**, *19*, 6538−6545. (b) Peng, X.; Yang, Z.; Wang, J.; Fan, J.; He, Y.; Song, F.; Wang, B.; Sun, S.; Qu, J.; Qi, J.; Yan, M. *J. Am. Chem. Soc.* **2011**, *133*, 6626−6635. (c) Zhang, S.; Wu, T.; Fan, J.; Li, Z.; Jiang, N.; Wang, J.; Dou, B.; Sun, S.; Song, F.; Peng, X. *Org. Biomol. Chem.* **2013**, *11*, 555−558. (d) Li, Z.; Sun, S.; Yang, Z.; Zhang, S.; Zhang, H.; Hu, M.; Cao, J.; Wang, J.; Liu, F.; Song, F.; Fan, J.; Peng, X. *Biomaterials* **2013**, *34*, 6473−6481.

(8) (a) Wen, X.; Yu, P.; Toh, Y.-R.; Hsu, A.-C.; Lee, Y.-C.; Tang, J. *J. Phys. Chem. C* **2012**, *116*, 19032−19038. (b) Goushi, K.; Yoshida, K.; Sato, K.; Adachi, C. *Nat. Photonics* **2012**, *6*, 253−258. (c) Uoyama, H.; Goushi, K.; Shizu, K.; Nomura, H.; Adachi, C. *Nature* **2012**, *492*, 234−238. (d) Mehes, G.; Nomura, H.; Zhang, Q.; Nakagawa, T.; Adachi, C. *Angew. Chem., Int. Ed. Engl.* **2012**, *51*, 11311−11315. (e) Tanaka, H.; Shizu, K.; Nakanotani, H.; Adachi, C. *Chem. Mater.* **2013**, *25*, 3766−3771.

(9) (a) Berberan-Santos, M. N.; Garcia, J. M. M. *J. Am. Chem. Soc.* **1996**, *118*, 9391−9394. (b) Deaton, J. C.; Switalski, S. C.; Kondakov, D. Y.; Young, R. H.; Pawlik, T. D.; Giesen, D. J.; Harkins, S. B.; Miller, A. J. M.; Mickenberg, S. F.; Peters, J. C. *J. Am. Chem. Soc.* **2010**, *132*, 9499−9508.

(10) (a) Bachilo, S. M.; Benedetto, A. F.; Weisman, R. B.; Nossal, J. R.; Billups, W. E. *J. Phys. Chem. A* **2000**, *104*, 11265−11269. (b) Endo, A.; Ogasawara, M.; Takahashi, A.; Yokoyama, D.; Kato, Y.; Adachi, C. *Adv. Mater.* **2009**, *21*, 4802−4806. (c) Zhang, Q.; Li, J.; Shizu, K.; Huang, S.; Hirata, S.; Miyazaki, H.; Adachi, C. *J. Am. Chem. Soc.* **2012**, *134*, 14706−14709. (d) Lee, J.; Shizu, K.; Tanaka, H.; Nomura, H.; Yasuda, T.; Adachi, C. *J. Mater. Chem. C* **2013**, *1*, 4599−4604. (e) Nasu, K.; Nakagawa, T.; Nomura, H.; Lin, C. J.; Cheng, C. H.;

Tseng, M. R.; Yasuda, T.; Adachi, C. *Chem. Commun.* **2013**, *49*, 10385−10387. (f) Nakagawa, T.; Ku, S. Y.; Wong, K. T.; Adachi, C. *Chem. Commun.* **2012**, *48*, 9580−9582.
(11) (a) Berden-Zrimec, M.; Drinovec, L.; Zrimec, A. *Chlorophyll a Fluorescence in Aquatic Sciences: Methods and Applications*; (a) Suggett, D. J., Borowitzka, M., Prášil, O., Eds.; Developments in Applied Phycology, Vol. *4*; Springer SBM: New York, 2010; pp 293−309. (b) Benniston, A. C.; Harriman, A.; Llarena, I.; Sams, C. A. *Chem. Mater.* **2007**, *19*, 1931−1938.
(12) Huang, Z.; Ji, D.; Xia, A.; Koberling, F.; Patting, M.; Erdmann, R. *J. Am. Chem. Soc.* **2005**, *127*, 8064−8066.
(13) (a) Scholz, M.; Dedic, R.; Breitenbach, T.; Hala, J. *Photochem. Photobiol. Sci.* **2013**, *12*, 1873−1884. (b) Yao, L.; Yang, B.; Ma, Y. *Sci. China: Chem.* **2014**, *57*, 335−345.
(14) Xiong, X.; Song, F.; Sun, S.; Fan, J.; Peng, X. *Asian J. Org. Chem.* **2013**, *2*, 145−149.
(15) (a) Bolton, O.; Lee, K.; Kim, H.-J.; Lin, K. Y.; Kim, J. *Nat. Chem.* **2011**, *3*, 205−210. (b) Li, L.; Zhao, Y.; Wu, Y.; Tong, A. *Talanta* **1998**, *46*, 1147−1154. (c) Lee, D.; Bolton, O.; Kim, B. C.; Youk, J. H.; Takayama, S.; Kim, J. *J. Am. Chem. Soc.* **2013**, *135*, 6325−6329.
(16) Zhang, G.; Chen, J.; Payne, S. J.; Kooi, S. E.; Demas, J. N.; Fraser, C. L. *J. Am. Chem. Soc.* **2007**, *129*, 8942−8943.
(17) (a) Sumiya, S.; Doi, T.; Shiraishi, Y.; Hirai, T. *Tetrahedron* **2012**, *68*, 690−696. (b) Magde, D.; Rojas, G. E.; Seybold, P. G. *Photochem. Photobiol.* **1999**, *70*, 737−744.
(18) (a) Yang, P.; Zhao, J.; Wu, W.; Yu, X.; Liu, Y. *J. Org. Chem.* **2012**, *77*, 6166−6178. (b) Guo, H.; Li, Q.; Ma, L.; Zhao, J. *J. Mater. Chem.* **2012**, *22*, 15757−15768. (c) Zhang, C.; Zhao, J.; Wu, S.; Wang, Z.; Wu, W.; Ma, J.; Guo, S.; Huang, L. *J. Am. Chem. Soc.* **2013**, *135*, 10566−10578. (d) Cui, X.; Charaf-Eddin, A.; Wang, J.; Le Guennic, B.; Zhao, J.; Jacquemin, D. *J. Org. Chem.* **2014**, *79*, 2038−2048.
(19) (a) DeRosa, M. C.; Crutchley, R. J. *Coord. Chem. Rev.* **2002**, *233*−*234*, 351−371. (b) Geissbuehler, M.; Spielmann, T.; Formey, A.; Marki, I.; Leutenegger, M.; Hinz, B.; Johnsson, K.; Van De Ville, D.; Lasser, T. *Adv. Exp. Med. Biol.* **2012**, *737*, 263−268. (c) Stromqvist, J.; Chmyrov, A.; Johansson, S.; Andersson, A.; Maler, L.; Widengren, J. *Biophys. J.* **2010**, *99*, 3821−3830.
(20) (a) Yang, N.; Cohen, A. E. *Opt. Express* **2010**, *18*, 25461−25467. (b) Mik, E. G.; Johannes, T.; Zuurbier, C. J.; Heinen, A.; Houben-Weerts, J. H.; Balestra, G. M.; Stap, J.; Beek, J. F.; Ince, C. *Biophys. J.* **2008**, *95*, 3977−3990. (c) Zhang, G.; Palmer, G. M.; Dewhirst, M. W.; Fraser, C. L. *Nat. Mater.* **2009**, *8*, 747−751.
(21) Grzywacz, J. *Nature* **1967**, *213*, 385−386.
(22) Galley, W. E. L. a. W. C. *Biophys. J.* **1988**, *54*, 627−635.
(23) Takase, M.; Narita, T.; Fujita, W.; Asano, M. S.; Nishinaga, T.; Benten, H.; Yoza, K.; Mullen, K. *J. Am. Chem. Soc.* **2013**, *135*, 8031−8040.
(24) (a) Kobayashi, A.; Takehira, K.; Yoshihara, T.; Uchiyama, S.; Tobita, S. *Photochem. Photobiol. Sci.* **2012**, *11*, 1368−1376. (b) Chen, H.; Jiang, Y.-B. *Chem. Phys. Lett.* **2000**, *325*, 605−609. (c) Gillbro, A. N. M. a. T. *J. Phys. Chem. A* **1998**, *102*, 5049−5058.
(25) Gu, L.; Hall, D. J.; Qin, Z.; Anglin, E.; Joo, J.; Mooney, D. J.; Howell, S. B.; Sailor, M. J. *Nat. Commun.* **2013**, *4*, 2326−2333.
(26) (a) Liu, Q.; Yin, B.; Yang, T.; Yang, Y.; Shen, Z.; Yao, P.; Li, F. *J. Am. Chem. Soc.* **2013**, *135*, 5029−5037. (b) Ogunsipe, A.; Nyokong, T. *Photochem. Photobiol. Sci.* **2005**, *4*, 510−516.